ARTICLE OPEN

Check for updates

Quantum storage of 1650 modes of single photons at telecom wavelength

Shi-Hai Wei[1,2], Bo Jing[1,7]✉, Xue-Ying Zhang[1], Jin-Yu Liao[1], Hao Li[3], Li-Xing You[3], Zhen Wang[3], You Wang[1,4], Guang-Wei Deng[1,5], Hai-Zhi Song[1,4], Daniel Oblak[6]✉, Guang-Can Guo[1,5] and Qiang Zhou[1,2,5]✉

To advance the full potential of quantum networks one should be able to distribute quantum resources over long distances at appreciable rates. As a consequence, all components in such networks need to have large multimode capacity to manipulate photonic quantum states. Towards this end, a photonic quantum memory with a large multimode capacity, especially one operating at telecom wavelength, remains an important challenge. Here we optimize the preparation of atomic frequency combs and demonstrate a spectro-temporally multiplexed quantum memory in a 10-m-long cryogenically cooled erbium doped silica fibre. Our multiplexing storage has five spectral channels - each 10 GHz wide with 5 GHz separation - with up to 330 temporal modes in each, thus resulting in a simultaneous storage of 1,650 modes of heralded single photons with a 1000-fold increasing in coincidence detection rate with respect to single mode storage. Our results could pave the way for high speed quantum networks compatible with the infrastructure of fibre optical communication.

npj Quantum Information (2024)10:19 ; https://doi.org/10.1038/s41534-024-00812-1

INTRODUCTION

Multimode capacity of communication channel is an essential requirement for high data rates in modern communication networks. Towards future quantum networks[1–4] compatible with existing telecom infrastructures, this requirement must also be applied[5,6]. One challenge in pursuing such a quantum network is to develop a multimode quantum memory[7–11], which is able to simultaneously store and process multiple modes of single photons in various degrees of freedom, such as in temporal degree[12–27], spectral degree[28–30], spatial degree[31–39], or any combination of these[40,41]. Overall the multimode capacity of a quantum memory is determined by the number of storage channels in spectral or spatial domain and the number of storage temporal modes in each storage channel.

To realize a large multimode quantum storage capacity, the use of multiple spatial channels has yielded a good performance, with a channel number up to 665 realized in gaseous atomic ensembles[36] based on Duan-Lukin-Cirac-Zoller (DLCZ) protocol[42]. Further improvement on the multimode capacity of such memory could be achieved via increasing the number of stored temporal modes in each of these channels. However, the storage of multiple temporal modes remains challenging in atomic gas ensembles due to limitations of the applied storage protocols[42–44]. Specifically, the number of temporal modes that can be stored is related to the optical depth (OD) of the storage media[45]. Fortunately, the atomic frequency comb (AFC) quantum memory with rare-earth ion-doped (REID) materials does not feature this constraint in terms of OD for the storage of multiple temporal modes[46], where the multimode capacity is proportional to the total number of teeth of the prepared AFCs[26], i.e., the product of channel number, storage time and the per bandwidth of AFC. Notable efforts have been devoted to improving the storage mode number of the AFC memory, such as increasing the ratio between storage time and temporal mode size[27], preparing multiple AFC channels by spectral multiplexing[28–30], and storing multiple degrees of freedom of single photons[41]. While an AFC quantum memory with 2500 teeth has been prepared[27], it is still challenging to demonstrate a quantum memory with an even larger multimode capacity.

Towards this end, we optimize the preparation of AFCs in five spectral channels with a total number of more than 10,000 teeth, and demonstrate a multimode storage of 1650 spectro-temporal modes of single photon at telecom wavelength with a piece of erbium doped silica fibre (EDF). Compared to single mode storage, we achieve a 1,000-fold increasing in coincidence detection rate. Our result could pave the way towards developing future quantum internet by utilizing multimode quantum memory compatible with the infrastructure of fibre optical communication system.

RESULTS

Multimode quantum storage scheme

Based on the inhomogeneous broadening in REID materials, an $Sn \times Tn$ multimode quantum memory can be realized by using Sn spectral channels and Tn temporal modes in each spectral channel (see Fig. 1a). Through spectral tailoring of the inhomogeneous broadened absorption line of REID materials, AFC channels with a number of Sn in the spectral domain are prepared. In each spectral channel, a train of single photons in Tn temporal modes are stored, with the maximum value of Tn determined by the time-bandwidth product of the AFC memory. By doing so, a total

[1]Institute of Fundamental and Frontier Sciences & School of Optoelectronic Science and Engineering, University of Electronic Science and Technology of China, Chengdu 610054, P. R. China. [2]Research Center for Quantum Internet, Tianfu Jiangri Laboratory, Chengdu 641419, P. R. China. [3]Shanghai Institute of Microsystem and Information Technology, Chinese Academy of Sciences, Shanghai 200050, P. R. China. [4]Southwest Institute of Technical Physics, Chengdu 610041, P. R. China. [5]CAS Key Laboratory of Quantum Information, University of Science and Technology of China, Hefei 230026, P. R. China. [6]Institute for Quantum Science and Technology, and Department of Physics & Astronomy, University of Calgary, 2500 University Dr. NW, Calgary, AB T2N 1N4, Canada. [7]Present address: School of Information Science and Technology, Southwest Jiaotong University, Chengdu 611756, P. R. China. ✉email: bjing@uestc.edu.cn; doblak@ucalgary.ca; zhouqiang@uestc.edu.cn

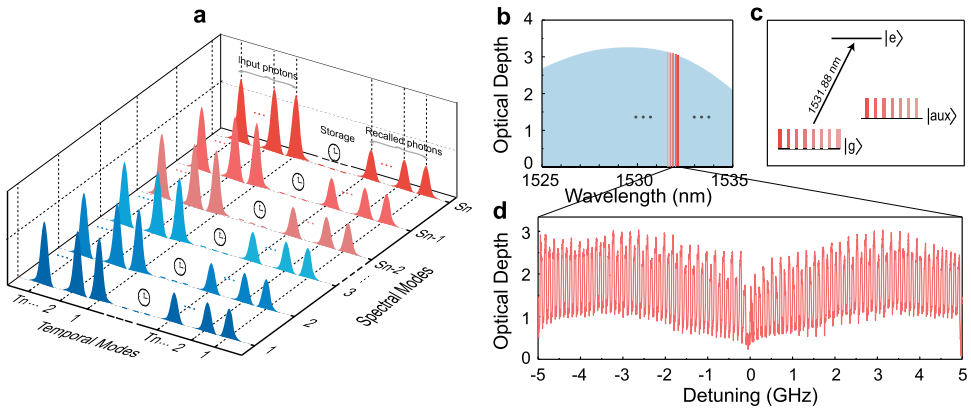

Fig. 1 Spectro-temporal multimode quantum storage of single photons at telecom wavelength. a General scheme for storage of $Sn \times Tn$ modes of single photons. A train of *Tn* temporal modes are stored into the AFCs with *Sn* spectral channels, resulting in storage of $Sn \times Tn$ modes of single photons. **b** The absorption profile of $^4I_{15/2}$ to $^4I_{13/2}$ transitions of Er^{3+} ions in the EDF at 10 mK. The inhomogeneous broadening is up to 2 THz (only 1 THz are shown here). In the section of inhomogeneous broadening absorption profile (70 GHz wide), we prepare five 10-GHz-wide AFCs with a separation of 5 GHz between the edges of adjacent AFCs. In principle, over seventy such AFCs can be prepared if we make use of the entire inhomogeneous broadening. **c** Simplified energy level scheme of Er^{3+} ions in erbium doped silica fibre. AFCs are prepared through frequency-selective optical pumping that transfers atomic states from the ground state ($|g\rangle$) to the auxiliary state ($|aux\rangle$) via the excited state ($|e\rangle$), forming AFCs. **d** A typical trace of 10-GHz-wide AFC measured in our experiment (the central wavelength of the AFC is 1532.00 nm, and comb spacing Δ is 100 MHz, leading to $T_{storage} = 10$ ns).

number of $Sn \times Tn$ modes of single photons are stored, simultaneously. To develop such a quantum memory with multimode capacity at telecom wavelength, a promising REID material is low doping concentration EDF, which has a telecom-band transition wavelength and THz-wide inhomogeneous broadening (see Fig. 1b, c).

Experimental setup

The experimental setup is composed of an EDF based AFC quantum memory with five spectral channels, a heralded single photon source at telecom wavelength, and a coincidence detection system, as illustrated in Fig. 2a. The experimental time sequences are also shown in Fig. 2b (see Methods).

We prepare an AFC quantum memory with five spectral channels in a 10-m-long EDF cooled to a temperature of 10 mK and exposed to a magnetic field of 2000 Gauss (see Fig. 2a(I) and Methods for details). More precisely, we propose and apply an approach - optical frequency comb combined with frequency chirping - to prepare five individual AFCs, each with a bandwidth of 10 GHz, at central wavelengths of 1532.11 nm, 1532.00 nm, 1531.88 nm, 1531.76 nm and 1531.65 nm, labeled as channels of 1, 2, 3, 4, and 5 (see Supplementary Note 1 for more details on preparing five AFCs by using optical frequency comb combined with frequency chirping method). Figure 1d depicts a typical AFC (channel 2) in our experiment, and all the five AFCs are shown in Supplementary Note 1. Note that different from using multiple individual lasers in parallel to prepare spectrally multiplexed AFC quantum memory[29], our method not only prepares such an AFC quantum memory by using a single laser, but also guarantees each channel with large bandwidth. Moreover, the scheme applies spectral isolation among channels, thus making the crosstalk among different storage channels to be negligible. When a single photon, matched with one of the AFCs, is absorbed by the AFC memory, the prepared Dicke state can be expressed as[47]:

$$|\Psi\rangle = \frac{1}{\sqrt{W}}(|1_1 0_2 0_3 \ldots 0_W\rangle + |0_1 1_2 0_3 \ldots 0_W\rangle + \ldots + |0_1 0_2 0_3 \ldots 1_W\rangle), \quad (1)$$

where W is the number of AFC tooth within the bandwidth of the single photon. Each tooth can be treated as a two-level system with collective states $|0\rangle$ and $|1\rangle$, in which $|0\rangle$ represents all atoms in the tooth are in the ground state, $|1\rangle$ represents that a single atom in the tooth is excited by the single photon. After the creation of the Dicke state, different terms in Eq. (1), begin to accumulate different phases, $e^{i\delta_j t}$, where $\delta_j = (j-1)\Delta$ $(j = 1, 2, \ldots, W)$ represents the relative detuning of the *jth* tooth to the first tooth, and Δ is the teeth spacing of AFC). At the time of $t = 1/\Delta$, the phases of all terms in the state are equal to an integer multiple of 2π, i.e., equivalent to 0. This process of rephasing leads to the re-emission of input photon in its original quantum state. In our scheme, we utilize spectro-temporally multiplexed storage to improve the stored mode number. For the temporal multiplexing quantum storage, the larger temporal mode number in each AFC channel corresponds to the Dicke state with more absorbers, i.e., the larger number of AFC teeth W, which would increase the fragility of the prepared Dicke state[47], resulting in the decreasing of storage efficiency. While for spectral multiplexing, different Dicke states are prepared at different detuning in inhomogeneous broadening of rare-earth ions, in which the number of absorbers for each state remains constant, preventing an increase in the fragility of the states.

To characterize the five spectral channels of quantum memory, we generate heralded single photons at telecom wavelength in a fibre pig-tailed periodically poled lithium niobate (PPLN) module[48–50], as shown in Fig. 2a(II). The light from a continuous-wave (CW) laser (PPCL300, PURE Photonics) operating at 1540.60 nm is modulated to light pulses and subsequently sent into the PPLN module. The cascaded second-harmonic generation (SHG) and spontaneous parametric down conversion (SPDC) processes result in correlated photon-pairs centred at 1540.60 nm with a bandwidth of ~60 nm. After efficient filtering, the central wavelengths of signal and idler photons are 1531.88 nm and 1549.32 nm with a bandwidth of ~100 GHz. The signal photons are sent into the five AFC spectral channels. It is worth noting that AFC itself is both a memory and a quantum information processor, which can also realize pulse sequencing, splitting, manipulating, filtering[51], etc. In our experiment, the spectral modes that do not match the storage bandwidth will be either absorbed and re-emitted spontaneously (with a decay time of ~10 ms) or pass through the memory, in which case they can be discriminated by their arrival time. Then, recalled signal photons from different AFCs are selected by a tunable fibre Bragg grating (FBG). The idler photons corresponding to different recalled signal photons are further selected by another FBG. The two FBGs enable the selective detection of different frequency modes employed in

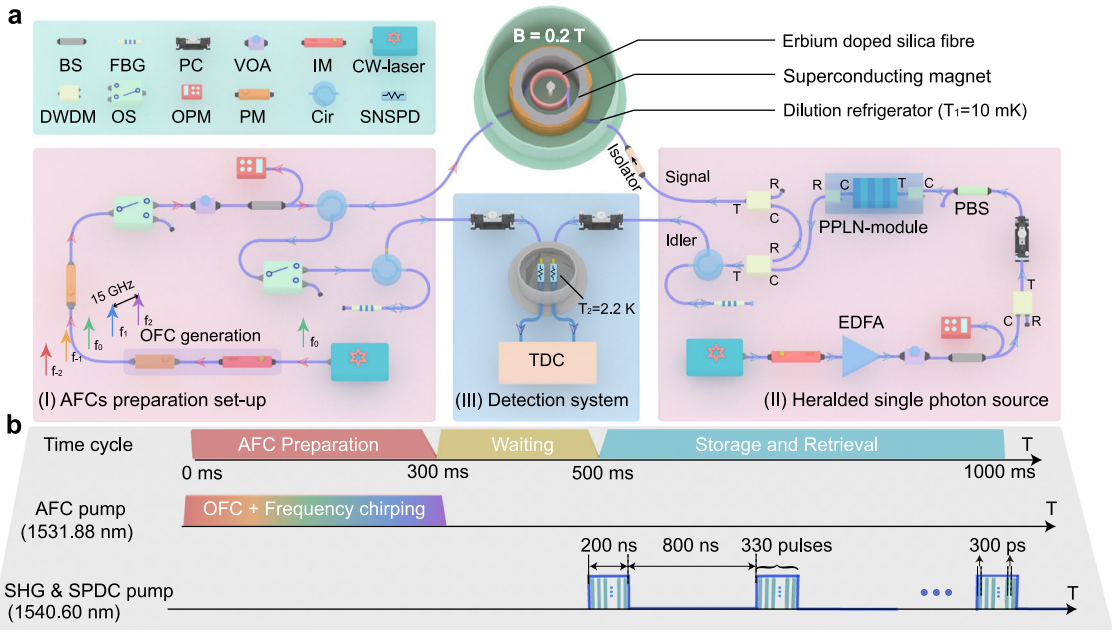

Fig. 2 Experimental setup and time sequences. a Experimental setup. (I) Preparation of AFC memory with five spectral channels. The erbium doped silica fibre (EDF) is cooled to a temperature of 10 mK by a dilution refrigerator and exposed to a magnetic field of 2000 Gauss provided by a superconducting magnet. Light from a continuous-wave laser (CW-laser) is firstly modulated to an optical frequency comb (OFC) by an intensity modulator (IM) and a phase modulator (PM). Then another PM is utilized to generate chirped light on each comb of the OFC. The modulated pump light is sent to the EDF via an optical circulator (Cir). Optical switch (OS) and variable optical attenuator (VOA) are used to control the pump time and intensity. Beam splitter (BS) and optical power meter (OPM) are utilized to monitor the pump light power. Fibre Bragg grating (FBG) is used to select signal photons recalled from different AFCs. (II) Preparation of the heralded single photon source (HSPS). Light from a CW-laser is modulated to 300 ps pulses by an IM and sent to the periodically poled lithium niobate (PPLN) module for generating correlated photon-pairs. By utilizing two dense wavelength division multiplexers (DWDMs), signal photons at 1531.88 nm and idler photons at 1549.32 nm with a bandwidth of 100 GHz are filtered out. FBG is used to select the idler photons corresponding to different spectral channels. Subsequently idler photons are directly sent to the detection system. The signal photons are sent into the EDF for storage. Erbium doped fibre amplifier (EDFA) and VOA are used to adjust the pump power. Polarization controller (PC) and polarizing beam splitter (PBS) are utilized to control the polarization of pump light. (III) Detection system. The idler and recalled signal photons are detected by two superconducting nanowire single photon detectors (SNSPDs). Coincidence measurements are performed by a time-to-digital converter (TDC). PCs are used to control the polarizations of signal and idler photons. **b** Time sequences. The cycle time of the experiment is one second, including 300 ms for AFCs preparation, 200 ms for waiting spontaneously emitted photons from excited states, and 500 ms for storage. The AFC pump laser is modulated to OFC and frequency chirped light within the preparation time of 300 ms. The SHG & SPDC pump laser with the repetition of 1 μs is modulated into 330 light pulses per cycle with pulse durations of and spaced by 300 ps (more details see Methods).

spectral multiplexing. In other words, each spectral channel can be individually discriminated and treated as an independent light-matter interface owing to the distinguishable signal photons and idler photons with different frequency, which is crucial for the development of spectral multiplexing quantum repeaters. It is worth noting that the transmission efficiency of FBG with the idler (signal) channel is 93% (89%). The bandwidth of the FBG is 0.06 nm for idler channel and 0.05 nm for signal channel. And the tuning speed of the FBG for each channel is around 20 s (see Supplementary Note 2 for more details of heralded single photon source).

Finally, we establish a coincidence detection system consisting of superconducting nanowire single photon detectors (SNSPDs, P-CS-6, PHOTEC Corp.) and a time-to-digital converter (TDC, quTAG, qutools), as shown in Fig. 2a(III) (see Methods for details of the SNSPDs). All SNSPD detection signals are delivered to the TDC to perform coincidence measurements. The system storage efficiency can be calculated by the ratio of the counts of recalled heralded photons to that of the input heralded photons. The second-order cross-correlation function ($g^{(2)}_{s,i}(0)$) between signal and idler photons after/before storage is calculated as:

$$g^{(2)}_{s,i}(0) = \frac{p_{si}}{p_s \cdot p_i}, \tag{2}$$

where p_{si} is the probability of 3-fold coincidence detections of trigger signal, idler photons, and signal photons, p_s (p_i) is the probability of coincidence detections of trigger signal and signal (idler) photons, respectively. Note that the coincidence detection in our experiment with trigger signal enables us to select the recalled photons by their arrival time, thus reducing the noise photon from the residual spontaneous emission. According to the Cauchy-Schwarz inequality[52], a non-classical field satisfies $g^{(2)}_{s,i}(0)>2$. More details of measuring $g^{(2)}_{s,i}(0)$ through coincidence counts are given in Methods.

Measurement

First, we investigate the performance of the five AFC spectral channels. To this end, we vary the storage time from 5 ns to 230 ns by programming by programming the AFC tooth number from 50 to 2300 in each channel. For each case, we map heralded single photons onto each of the five spectral channels, and subsequently collect coincidence statistics of the recalled photons to gauge storage performance in terms of storage time, efficiency, and preservation of quantum properties manifested in the $g^{(2)}_{s,i}(0)$ values. According to the measured results, the system storage efficiency of each channel with different storage times ranges from 0.1% to 1%. The $g^{(2)}_{s,i}(0)$ still remains above 25 for the maximum storage time of 230 ns (see Table 1), demonstrating strong non-classical properties for all storage times (see Supplementary Note 3, 4 and 5 for more analysis of the storage efficiency and $g^{(2)}_{s,i}(0)$ for five individual AFCs). Furthermore, these measurements demonstrate that our memory, in principle, is able to

Table 1. Measured crosstalk ($g^{(2)}_{s,i}(0)$) between recalled signal photons and idler photons with different storage time.

Storage time	Channel 1	Channel 2	Channel 3	Channel 4	Channel 5
0 ns	25.64 ± 0.19	27.53 ± 0.18	27.91 ± 0.18	28.38 ± 0.18	28.62 ± 0.19
10 ns	26.13 ± 1.45	28.97 ± 1.20	26.81 ± 1.49	26.10 ± 1.05	27.07 ± 1.15
50 ns	26.95 ± 1.48	26.72 ± 1.32	26.85 ± 1.59	26.95 ± 1.23	22.99 ± 1.11
100 ns	26.08 ± 1.90	25.77 ± 1.60	24.48 ± 1.92	27.01 ± 1.69	25.85 ± 1.36
230 ns	26.22 ± 4.32	31.00 ± 4.41	26.22 ± 4.32	26.59 ± 3.81	22.09 ± 3.34

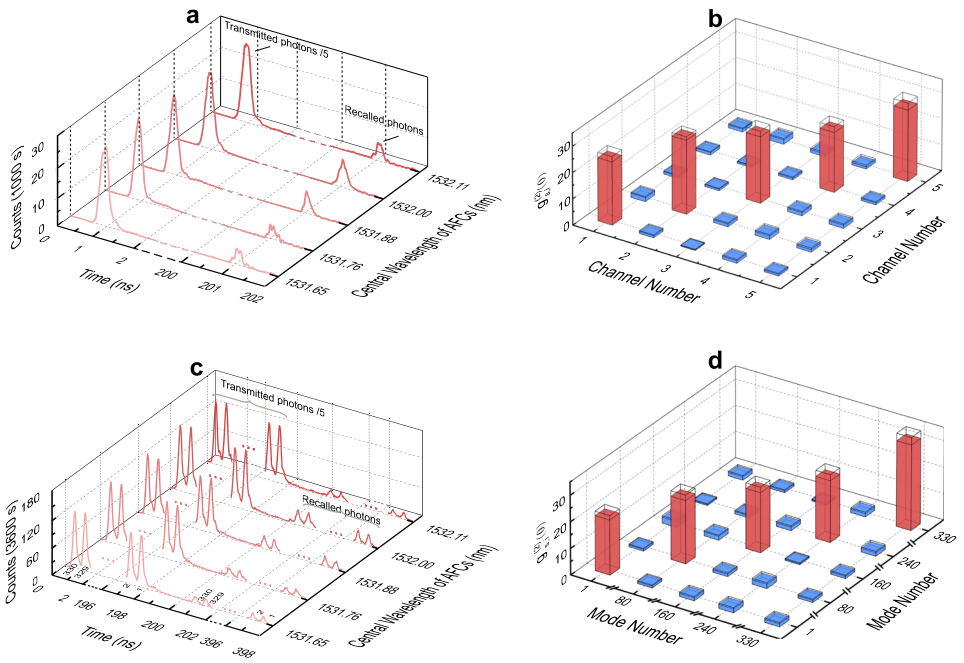

Fig. 3 Characterization for the multimode quantum memory. a Results for spectral-multiplexed storage in five AFC spectral channels with a storage time of 200 ns. The integration time is 1000 s. **b** Crosstalk between different spectral modes of idler photons and recalled photons. The average measured $g^{(2)}_{s,i}(0)$ between recalled photons and idler photons is 25.48 ± 1.05 for 5 correlated spectral modes and 1.01 ± 0.10 for 20 uncorrelated modes. **c** Results for storage of 1650 spectro-temporal modes of single photons at telecom wavelength. Heralded single photons with 330 temporal modes are generated and stored into five spectral channels with a storage time of 200 ns, totally, 1650 modes are stored into the five AFCs. The integration time is 1000 s. **d** Crosstalk between different temporal modes of idler photons and signal photons recalled from channel 2 (mode numbers: 1, 80, 160, 240, 330). The average $g^{(2)}_{s,i}(0)$ between correlated recalled signal and idler photon modes (1650 pairs) is 22.92 ± 0.07. For uncorrelated modes, the average $g^{(2)}_{s,i}(0)$ is 1.01 ± 0.01. Error bars in Figs. (**b**) and (**d**) are calculated by standard deviations of counts which obey Poisson distribution.

perform quantum storage of 920 temporal modes of telecom-band single photons in each spectral channel. The temporal mode number is calculated by 10 GHz × 230 ns/2.5, where the factor of 2.5 is from the Nyquist-Shannon sampling theorem[26]. With five parallel channels, the total multimode capacity reaches 4600 in our demonstration.

Second, to examine the effect of crosstalk between different spectral channels, we measure the $g^{(2)}_{s,i}(0)$ between recalled signal photons and heralding idler photons corresponding to different spectral channels[37]. If there is no crosstalk between different spectral channels, the measured $g^{(2)}_{s,i}(0)$ between uncorrelated channels should be around 1. On the other hand, with increasing crosstalk, the value of $g^{(2)}_{s,i}(0)$ would also increase (the relationship between crosstalk and $g^{(2)}_{s,i}(0)$ is shown in Supplementary Note 6). To eliminate the crosstalk between spectral channels, a sufficiently large separation between adjacent AFCs is required[28] - in our case we choose 5 GHz separation. We first assess the crosstalk resulting from the source and detection system without the quantum memory. For the crosstalk characterization, we label the signal photons corresponding to channels 1 to 5 as $S_1, S_2, \ldots, S_5$, and similarly, the idler photons as $I_1, I_2, \ldots, I_5$. The choice of which signal and idler channels to detect is determined by the tunable FBG filter settings. Measuring coincidences between S_m and I_n, where $m, n \in \{1, 2, 3, 4, 5\}$, we calculate a 5×5 matrix of $g^{(2)}_{s,i}(0)$. The measured average $g^{(2)}_{s,i}(0)$ is 27.90 ± 0.18 for 5 pairs of correlated spectral modes ($m = n$) and 1.07 ± 0.02 for the 20 pairs of uncorrelated spectral modes ($m \neq n$), where error bars are acquired through Monte Carlo simulation. The detailed values are shown in Supplementary Note 7. The results indicate that the crosstalk between different spectral channels is negligible. Next, we evaluate whether the multimode memory induces additional crosstalk. To that end, we send the signal photons into the five AFC spectral channels with the storage time of 200 ns. The recalled signal photons from different channels are indexed as $R_1, R_2, \ldots, R_5$. Measuring coincidences between R_m and I_n, we obtain the recalled signal photons from five channels (see Fig. 3a).

The measured coincidences detection rates of idler photon and recalled signal photons after storage are 0.19 ± 0.01 Hz, 0.36 ± 0.02 Hz, 0.29 ± 0.02 Hz, 0.21 ± 0.01 Hz, and 0.20 ± 0.01 Hz, respectively. The transmitted photons output from the EDF indicate the optical delay of the fibre, and the time delay between the transmitted photons and the recalled photons shows the storage time of the AFC memory. We again calculate the 5×5 array of $g^{(2)}_{s,i}(0)$ values as shown in Fig. 3b. The measured average $g^{(2)}_{s,i}(0)$ between recalled photons and idler photons is 25.48 ± 1.05 for five correlated spectral modes and 1.01 ± 0.10 for 20 pairs of uncorrelated spectral modes. The results confirm that the crosstalk between different spectral channels is negligible in our quantum memory.

Third, to quantify the storage mode number of our quantum memory, we create a train of heralded single photons - with pulse durations of and spaced by 300 ps - for simultaneous storage in all five spectral channels. With the storage time of 200 ns, 330 temporal modes are simultaneously stored in each spectral channel (see Fig. 3c). The measured coincidence detection rates of idler photon and signal photons after storage are 37.18 ± 6.10 Hz, 67.52 ± 8.22 Hz, 69.31 ± 8.33 Hz, 44.13 ± 6.64 Hz, and 39.16 ± 06.26 Hz, respectively. Compared to single mode storage, it is around 200-fold increasing in coincidence detection rate for each spectral channel. Noting that the detection rate of temporal multimode storage should be 330 times higher than that of single-mode storage, but due to the effect of the dead time of SNSPDs (~50 ns), the coincidence rate of the multimode storage drops with the mode number. The total stored mode number is, thus, up to 1650. Furthermore, to assess the crosstalk between different temporal modes, we obtain 1650×1650 values of $g^{(2)}_{s,i}(0)$ through measuring cross-correlation function between different idler photons and recalled signal photons. Figure 3d presents parts of $g^{(2)}_{s,i}(0)$ corresponding to different temporal modes in channel 2 (the full 1650×1650 array of $g^{(2)}_{s,i}(0)$ is shown in Supplementary Note 8). The average $g^{(2)}_{s,i}(0)$ between correlated signal and idler photonic modes (1650 pairs) is 22.92 ± 0.07, verifying that the non-classical correlations are intact. For uncorrelated modes the $g^{(2)}_{s,i}(0)$ is 1.01 ± 0.01 on average with error bar from Monte Carlo simulation, confirming the negligible crosstalk between different temporal modes. In addition, we conclude the key metrics of our multimode quantum memory in Table 2, which also includes the state-of-the-art of multimode quantum storage of non-classical light based on REID materials.

Table 2. Comparison on the time-bandwidth product and storage mode number of quantum memories for non-classical light based on different REID materials.

System	λ[a] (nm)	$T_{storage}$[b] (ns)	BW[c] (GHz)	TBP[d]	N[e]
$Eu^{3+}:Y_2SiO_5$[20]	580	1×10^6	0.002	2000	12
$Pr^{3+}:Y_2SiO_5$[41]	606	3500	0.06	210	135
$Tm^{3+}:Ti^{3+}:LiNbO_3$[64]	795	7	5	35	≥10
$Tm^{3+}:Y_3Al_5O_{12}$[65]	795	100	0.5	50	125
$Nd^{3+}:YVO_4$[17]	880	500	0.5	250	100
$Nd^{3+}:Y_2SiO_5$[66]	883	200	0.12	24	20
$Yb^{3+}:Y_2SiO_5$[27]	979	2.5×10^4	0.1	2500	1250
$Er^{3+}:Ti^{3+}:LiNbO_3$[67]	1532	48	6	288	96
$Er^{3+}:LiNbO_3$[68]	1532	100	4	400	147
EDF[29]	1532	50	16	800	48
$Er^{3+}:Y_2SiO_5$[59]	1536	1936	0.2	387.2	484
EDF (this work)	1532	230	50	11,500	1650

[a]λ is the wavelength of the stored single photons.
[b]$T_{storage}$ is the storage time of AFC quantum memory.
[c]BW is the available storage bandwidth of quantum memory.
[d]TBP is the time-bandwidth product of quantum memory.
[e]Number of stored modes, which is the product of the spectral channel number and the ratio between the storage time and the mode size.

DISCUSSION

An important feature of our demonstration is the large multimode capacity of quantum memory for the storage of single photons at telecom wavelength. Towards a memory with much larger multimode capacity in the future, it is necessary to further increasing the number of storage channel and its storage time[18]. In our demonstration, one could make using of entire THz-wide inhomogeneous broadening of the EDF to prepare more individual AFCs by using a broader optical frequency comb[53]. The storage time of AFC quantum memory could be increased by reducing its teeth spacing Δ, which is currently limited by our laser system - with a frequency drift of several MHz - for the AFC preparation. Furthermore, Δ will be limited by the linewidth AFC tooth, which is mainly determined by the spectral diffusion and the superhyperfine broadening of Er^{3+} ions. This needs to be further optimized by modifying the doping concentration of Er^{3+} ions and the co-dopant Al^{3+} ions in fibre[54,55]. Besides, full multimode operation is crucial for multiplexed quantum repeaters, which necessitates multimode heralding, storage, and detection. In our proof of principle demonstration, the heralding and detection are performed for each mode separately which is selected and characterized with FBGs and SNSPDs. A full multimode operation could be achieved by using more FBGs and SNSPDs.

Other upgrades could be applied to the EDF based quantum memories towards quantum networks. It is also possible to develop an on-demand quantum memory with spin-wave storage with a long-lived hyperfine level in a piece of EDF. However, it stays a challenge to discriminate the hyperfine levels in erbium ions without nuclear spin[56]. Fortunately, hyperfine levels with a coherence time of 380 microseconds with zero magnetic field[57] and 1.3 s with 7 T magnetic field[58] have been observed with $^{167}Er^{3+}$ ions doped in yttrium orthosilicate. An AFC-based quantum storage of entangled photons has also been implemented in $^{167}Er^{3+}:Y_2SiO_5$[59]. These results show a great potential for an on-demand spin-wave quantum storage with $^{167}Er^{3+}$ ions. Therefore, it could be a promising avenue to develop spin-wave storage by using $^{167}Er^{3+}$ ions doped fibre. In the on-demand configuration, the small spin-level splitting would limit the bandwidth of AFC channel, thus reducing the multimode capacity. However, spectro-temporal multiplexing can also ensure the on-demand storage with large multimode capacity. Applying spectral multiplexing can increase the number of AFC channels at different atomic detuning in large inhomogeneous broadening, in which each AFC can achieve spin-wave storage independently, thus increasing the spectral multimode capacity. Combined with the intrinsic temporal multimode capacity of AFC protocol, it is promising to achieve on-demand storage with large multimode capacity at telecom wavelength. With regards to the storage efficiency, the non-zero background absorption (d_0) of the prepared AFC is one of main limits. The d_0 is caused by the limited ratio of the lifetime of Zeeman sublevels (~300 ms) to the waiting time following the AFC preparation (200 ms). The lifetime of Zeeman sublevels could be extended by optimizing the doping concentration[6]. The trade-off between the waiting time and the signal-to-noise ratio (SNR) of the memory can be further investigated. It is also worth to note that an impedance-matched optical cavity could be applied to improve the storage efficiency[60,61]. Towards a

high-performance AFC quantum memory in the EDF, we propose a promising scheme to realize an impedance-matched quantum memory in a piece of optimized EDF (more details see Supplementary Note 9).

In summary, we have demonstrated a multimode quantum memory that is suitable for storage of spectro-temporal modes of single photons at telecom band. Our quantum memory with five 10-GHz wide AFCs channels allows for the storage of 1650 modes of heralded single photons - a 1000-fold increasing in coincidence detection rate compared to the single mode. Our results show that with the promising improvements on storage time and storage efficiency, the EDF based AFC quantum memory will pave the way for constructing quantum internet with the installed infrastructures of optical communication system.

METHODS

Erbium doped silica fibre

The experiment utilizes a 10-m-long, single-mode, commercial EDF with Er^{3+} ions doping concentration of 200 ppm, co-doped with Al, Ge, and P. The fibre is spooled to a home-made copper cylinder with a diameter of 4 cm and fixed in the dilution refrigerator (LD400, Bluefors), in which the temperature can be cooled below 10 mK. The measured absorption at 1532 nm is 0.35 dB/m at $T = 10$ mK. The EDF is fused with single-mode fibres for each end, and is exposed to 2000 Gauss magnetic field, the strength of which is optimized by observing the lifetime of Zeeman sublevels of $^4I_{15/2}$ level. With a magnetic field of 0.2 T, the lifetime reaches 0.278 ± 0.035 s, which ensures the persistent time of AFC (see Supplementary Note 10 for details). On the other hand, the applied magnetic field can eliminate a part of magnetic two-level systems, thus increasing the optical coherence time of erbium ions[62]. The loss of the whole fibre sample is about 2.5 dB, including bending, splicing, and transmission loss.

Experimental time sequences and procedures

The time sequences are shown in Fig. 2b. During the preparation time of 300 ms, the pump light from a CW-laser operating at 1531.88 nm is prepared into an optical frequency comb with frequency spacing of 15 GHz by an IM and a PM, both of which are driven by 15 GHz microwave signals. The optical frequency comb is sent to another PM, which is driven by an arbitrary waveform generator (AWG) to continuously generate frequency chirping light on each comb ranging from −5 GHz to 5 GHz (total span of 10 GHz). Then the prepared pump light is modulated into 300-ms-long light pulses by an OS, and sent into the EDF to prepare quantum memory with five spectral channels. The setting 200 ms waiting time is to decrease the influence of spontaneously emitted photons from excited ions on the recalled photons from the AFC (see Supplementary Note 11 for more details). During the storage time of 500 ms, another OS turns on. The light from a CW-laser operating at 1540.60 nm is modulated into a light pulse with pulse duration of 300 ps and the repetition rate of 1 MHz (for multiple temporal modes storage, the laser is modulated to 330 light pulses within one cycle of 1 μs, i.e., $T_{period} = 1$ μs) and sent to PPLN module for the generation of correlated photon-pairs with a bandwidth of ~60 nm. By utilizing DWDMs, signal photons at 1531.88 nm and idler photons at 1549.32 nm with a bandwidth of 100 GHz are filtered out. The signal photons are sent into five-channel quantum memory to filter and to store. After the storage time of $T_{storage}$, the signal photons are recalled from AFCs. Finally, the idler photons and recalled signal photons corresponding to different channels are selected by FBGs and detected by SNSPDs, subsequently performed coincidence analysis in the TDC.

Superconducting nanowire single photon detectors

All detections of single photons are carried out by a set of SNSPDs system provided by PHOTEC Corp. The system consists of SNSPD devices, cryostat system, and electronic control system. The niobium nitride (NbN) SNSPDs, manufactured by Shanghai Institute of Microsystem and Information Technology (SIMIT), operate at ~2.2 K in the cryostat system with a dark counting rate of ~100 Hz and a time jitter of ~100 ps. All detectors have a dead time of less than 50 ns and a detection efficiency of ~60%.

Calculation of cross-correlation function $g^{(2)}_{s,i}(0)$

Considering the counting effective events in m experimental trials, we record the total 3-fold coincidence counts C_{si} of the trigger signal, idler and signal photons, the coincidence counts C_s (C_i) between signal (idler) photons and trigger signals. With the photon detected probability in each trial calculated as $p_{si} = C_{si}/m$, $p_s = C_s/m$, $p_i = C_i/m$, the second-order cross-correlation function $g^{(2)}_{s,i}(0)$ is calculated by

$$g^{(2)}_{s,i}(0) = \frac{p_{si}}{p_s \cdot p_i} = \frac{C_{si} \cdot m}{C_s \cdot C_i}. \tag{3}$$

It is a strong indication of quantum correlations for photons-pairs if $g^{(2)}_{s,i}(0) \gg 2$. According to Cauchy-Schwarz inequality, it also indicates that the auto-correlation function of heralded signal photons is $\ll 1$, i.e., these signal photons are denoted as single photons[63]. For all the coincidence measurements in this paper, the width of coincidence window is 600 ps.

DATA AVAILABILITY

The data that support the findings of this study are available from the corresponding author on reasonable request.

Received: 3 February 2023; Accepted: 12 January 2024;
Published online: 01 February 2024

REFERENCES

1. Kimble, H. J. The quantum internet. *Nature* **453**, 1023–1030 (2008).
2. Simon, C. Towards a global quantum network. *Nat. Photonics* **11**, 678–680 (2017).
3. Wehner, S., Elkouss, D. & Hanson, R. Quantum internet: a vision for the road ahead. *Science* **362**, eaam9288 (2018).
4. Wei, S.-H. et al. Towards real-world quantum networks: a review. *Laser Photonics Rev.* **16**, 2100219 (2022).
5. Jin, J. et al. Telecom-wavelength atomic quantum memory in optical fiber for heralded polarization qubits. *Phys. Rev. Lett.* **115**, 140501 (2015).
6. Saglamyurek, E. et al. Quantum storage of entangled telecom-wavelength photons in an erbium-doped optical fibre. *Nat. Photonics* **9**, 83–87 (2015).
7. Collins, O., Jenkins, S., Kuzmich, A. & Kennedy, T. Multiplexed memory-insensitive quantum repeaters. *Phys. Rev. Lett.* **98**, 060502 (2007).
8. Simon, C. et al. Quantum repeaters with photon pair sources and multimode memories. *Phys. Rev. Lett.* **98**, 190503 (2007).
9. Lvovsky, A. I., Sanders, B. C. & Tittel, W. Optical quantum memory. *Nat. Photonics* **3**, 706–714 (2009).
10. Simon, C. et al. Quantum memories. *Eur. Phys. J. D* **58**, 1–22 (2010).
11. Heshami, K. et al. Quantum memories: emerging applications and recent advances. *J. Mod. Optic.* **63**, 2005–2028 (2016).
12. De Riedmatten, H., Afzelius, M., Staudt, M. U., Simon, C. & Gisin, N. A solid-state light–matter interface at the single-photon level. *Nature* **456**, 773–777 (2008).
13. Usmani, I., Afzelius, M., De Riedmatten, H. & Gisin, N. Mapping multiple photonic qubits into and out of one solid-state atomic ensemble. *Nat. Commun.* **1**, 12 (2010).
14. Bonarota, M., Le Gouët, J. & Chaneliere, T. Highly multimode storage in a crystal. *New J. Phys.* **13**, 013013 (2011).
15. Hosseini, M., Sparkes, B. M., Campbell, G., Lam, P. K. & Buchler, B. C. High efficiency coherent optical memory with warm rubidium vapour. *Nat. Commun.* **2**, 174 (2011).

16. Gündoğan, M., Mazzera, M., Ledingham, P. M., Cristiani, M. & de Riedmatten, H. Coherent storage of temporally multimode light using a spin-wave atomic frequency comb memory. *New J. Phys.* **15**, 045012 (2013).
17. Tang, J.-S. et al. Storage of multiple single-photon pulses emitted from a quantum dot in a solid-state quantum memory. *Nat. Commun.* **6**, 8652 (2015).
18. Jobez, P. et al. Towards highly multimode optical quantum memory for quantum repeaters. *Phys. Rev. A* **93**, 032327 (2016).
19. Tiranov, A. et al. Temporal multimode storage of entangled photon pairs. *Phys. Rev. Lett.* **117**, 240506 (2016).
20. Laplane, C., Jobez, P., Etesse, J., Gisin, N. & Afzelius, M. Multimode and long-lived quantum correlations between photons and spins in a crystal. *Phys. Rev. Lett.* **118**, 210501 (2017).
21. Wen, Y. et al. Multiplexed spin-wave–photon entanglement source using temporal multimode memories and feedforward-controlled readout. *Phys. Rev. A* **100**, 012342 (2019).
22. Heller, L., Farrera, P., Heinze, G. & de Riedmatten, H. Cold-atom temporally multiplexed quantum memory with cavity-enhanced noise suppression. *Phys. Rev. Lett.* **124**, 210504 (2020).
23. Liu, X. et al. Heralded entanglement distribution between two absorptive quantum memories. *Nature* **594**, 41–45 (2021).
24. Lago-Rivera, D., Grandi, S., Rakonjac, J. V., Seri, A. & de Riedmatten, H. Telecom-heralded entanglement between multimode solid-state quantum memories. *Nature* **594**, 37–40 (2021).
25. Su, M.-X. et al. On-demand multimode optical storage in a laser-written on-chip waveguide. *Phys. Rev. A* **105**, 052432 (2022).
26. Ortu, A. et al. Multimode capacity of atomic-frequency comb quantum memories. *Quantum Sci. Technol.* **7**, 035024 (2022).
27. Businger, M. et al. Non-classical correlations over 1250 modes between telecom photons and 979-nm photons stored in 171yb3+: Y2sio5. *Nat. Commun.* **13**, 1–8 (2022).
28. Sinclair, N. et al. Spectral multiplexing for scalable quantum photonics using an atomic frequency comb quantum memory and feed-forward control. *Phys. Rev. Lett.* **113**, 053603 (2014).
29. Saglamyurek, E. et al. A multiplexed light-matter interface for fibre-based quantum networks. *Nat. Commun.* **7**, 11202 (2016).
30. Askarani, M. F. et al. Long-lived solid-state optical memory for high-rate quantum repeaters. *Phys. Rev. Lett.* **127**, 220502 (2021).
31. Lan, S.-Y. et al. A multiplexed quantum memory. *Opt. Express* **17**, 13639–13645 (2009).
32. Grodecka-Grad, A., Zeuthen, E. & Sørensen, A. S. High-capacity spatial multimode quantum memories based on atomic ensembles. *Phys. Rev. Lett.* **109**, 133601 (2012).
33. Nicolas, A. et al. A quantum memory for orbital angular momentum photonic qubits. *Nat. Photonics* **8**, 234–238 (2014).
34. Ding, D.-S. et al. Quantum storage of orbital angular momentum entanglement in an atomic ensemble. *Phys. Rev. Lett.* **114**, 050502 (2015).
35. Zhou, Z.-Q. et al. Quantum storage of three-dimensional orbital-angular-momentum entanglement in a crystal. *Phys. Rev. Lett.* **115**, 070502 (2015).
36. Parniak, M. et al. Wavevector multiplexed atomic quantum memory via spatially-resolved single-photon detection. *Nat. Commun.* **8**, 2140 (2017).
37. Pu, Y. et al. Experimental realization of a multiplexed quantum memory with 225 individually accessible memory cells. *Nat. Commun.* **8**, 15359 (2017).
38. Chrapkiewicz, R., Dabrowski, M. & Wasilewski, W. High-capacity angularly multiplexed holographic memory operating at the single-photon level. *Phys. Rev. Lett.* **118**, 063603 (2017).
39. Tian, L. et al. Spatial multiplexing of atom-photon entanglement sources using feedforward control and switching networks. *Phys. Rev. Lett.* **119**, 130505 (2017).
40. Yang, T.-S. et al. Multiplexed storage and real-time manipulation based on a multiple degree-of-freedom quantum memory. *Nat. Commun.* **9**, 3407 (2018).
41. Seri, A. et al. Quantum storage of frequency-multiplexed heralded single photons. *Phys. Rev. Lett.* **123**, 080502 (2019).
42. Duan, L.-M., Lukin, M. D., Cirac, J. I. & Zoller, P. Long-distance quantum communication with atomic ensembles and linear optics. *Nature* **414**, 413–418 (2001).
43. Turukhin, A. et al. Observation of ultraslow and stored light pulses in a solid. *Phys. Rev. Lett.* **88**, 023602 (2001).
44. Reim, K. et al. Towards high-speed optical quantum memories. *Nat. Photonics* **4**, 218–221 (2010).
45. Nunn, J. et al. Multimode memories in atomic ensembles. *Phys. Rev. Lett.* **101**, 260502 (2008).
46. Afzelius, M., Simon, C., De Riedmatten, H. & Gisin, N. Multimode quantum memory based on atomic frequency combs. *Phys. Rev. A* **79**, 052329 (2009).
47. Zarkeshian, P. et al. Entanglement between more than two hundred macroscopic atomic ensembles in a solid. *Nat. Commun.* **8**, 906 (2017).
48. Lefebvre, P. et al. Compact energy–time entanglement source using cascaded nonlinear interactions. *J. Opt. Soc. Am. B* **38**, 1380–1385 (2021).
49. Zhang, Z. et al. High-performance quantum entanglement generation via cascaded second-order nonlinear processes. *npj Quantum Inform.* **7**, 123 (2021).
50. Yu, H. et al. Spectrally multiplexed indistinguishable single-photon generation at telecom-band. *Photonics Res.* **10**, 1417–1429 (2022).
51. Saglamyurek, E. et al. An integrated processor for photonic quantum states using a broadband light–matter interface. *New J. Phys.* **16**, 065019 (2014).
52. Chou, C., Polyakov, S., Kuzmich, A. & Kimble, H. Single-photon generation from stored excitation in an atomic ensemble. *Phys. Rev. Lett.* **92**, 213601 (2004).
53. Fortier, T. & Baumann, E. 20 years of developments in optical frequency comb technology and applications. *Commun. Phys.* **2**, 153 (2019).
54. Veissier, L. et al. Optical decoherence and spectral diffusion in an erbium-doped silica glass fiber featuring long-lived spin sublevels. *Phys. Rev. B* **94**, 195138 (2016).
55. Staudt, M. U. et al. Investigations of optical coherence properties in an erbium-doped silicate fiber for quantum state storage. *Opt. Commun.* **266**, 720–726 (2006).
56. Baldit, E. et al. Identification of Λ-like systems in Er^{3+}:Y_2SiO_5 and observation of electromagnetically induced transparency. *Phys. Rev. B* **81**, 144303 (2010).
57. Rakonjac, J. V. et al. Entanglement between a telecom photon and an on-demand multimode solid-state quantum memory. *Phys. Rev. Lett.* **127**, 210502 (2021).
58. Rančić, M., Hedges, M. P., Ahlefeldt, R. L. & Sellars, M. J. Coherence time of over a second in a telecom-compatible quantum memory storage material. *Nat. Phys.* **14**, 50–54 (2018).
59. Jiang, M.-H. et al. Quantum storage of entangled photons at telecom wavelengths in a crystal. *Nat. Commun.* **14**, 6995 (2023).
60. Afzelius, M. & Simon, C. Impedance-matched cavity quantum memory. *Phys. Rev. A* **82**, 022310 (2010).
61. Moiseev, S. A., Andrianov, S. N. & Gubaidullin, F. F. Efficient multimode quantum memory based on photon echo in an optimal qed cavity. *Phys. Rev. A* **82**, 022311 (2010).
62. Macfarlane, R., Sun, Y., Sellin, P. & Cone, R. Optical decoherence in Er^{3+}-doped silicate fiber: evidence for coupled spin-elastic tunneling systems. *Phys. Rev. Lett.* **96**, 033602 (2006).
63. Bashkansky, M., Vurgaftman, I., Pipino, A. C. & Reintjes, J. Significance of heralding in spontaneous parametric down-conversion. *Phys. Rev. A* **90**, 053825 (2014).
64. Saglamyurek, E. et al. Broadband waveguide quantum memory for entangled photons. *Nature* **469**, 512–515 (2011).
65. Davidson, J. H., Lefebvre, P., Zhang, J., Oblak, D. & Tittel, W. Improved light-matter interaction for storage of quantum states of light in a thulium-doped crystal cavity. *Phys. Rev. A* **101**, 042333 (2020).
66. Clausen, C. et al. Quantum storage of photonic entanglement in a crystal. *Nature* **469**, 508–511 (2011).
67. Askarani, M. F. et al. Storage and reemission of heralded telecommunication-wavelength photons using a crystal waveguide. *Phys. Rev. Appl.* **11**, 054056 (2019).
68. Zhang, X.-Y. et al. Storage of 147 temporal modes of telecom-band single photon with fiber-pigtailed Er^{3+}:$LiNbO_3$ waveguide. In *CLEO: Science and Innovations*, JTh6A–9 (Optica Publishing Group, 2022).

ACKNOWLEDGEMENTS

This work was supported by the National Key Research and Development Program of China (Nos. 2018YFA0307400, 2018YFA0306102), National Natural Science Foundation of China (Nos. 61775025, 91836102, U19A2076, 12004068), Innovation Program for Quantum Science and Technology (No. 2021ZD0301702), Sichuan Science and Technology Program (Nos. 2021YFSY0062, 2021YFSY0063, 2021YFSY0064, 2022YFSY0061, 2022YFSY0063, 2023YFSY0058, 2023YFSY0060), China Postdoctoral Science Foundation (Nos. 2020M683275, 2021T140093).

AUTHOR CONTRIBUTIONS

D.O., G.G., and Q.Z. conceived and supervised the project. S.W. and B.J. mainly carried out the experiment and collected the experimental data with help of other authors. H.L., L.Y. and Z.W. developed and maintained the SNSPDs used in the experiment. S.W., B.J. and Q.Z. analyzed the data. S.W., B.J., D.O. and Q.Z. wrote the manuscript with inputs from all other authors. All authors have given approval for the final version of the manuscript.

COMPETING INTERESTS

The authors declare no competing interests.

ADDITIONAL INFORMATION

Supplementary information The online version contains supplementary material available at https://doi.org/10.1038/s41534-024-00812-1.

Correspondence and requests for materials should be addressed to Bo Jing, Daniel Oblak or Qiang Zhou.

Reprints and permission information is available at http://www.nature.com/reprints

Publisher's note Springer Nature remains neutral with regard to jurisdictional claims in published maps and institutional affiliations.